AIAA JOURNAL
Vol. 33, No. 11, November 1995

Full and von Kármán Geometrically Nonlinear Analyses of Laminated Cylindrical Panels

Deokjoo Kim* and Reaz A. Chaudhuri†
University of Utah, Salt Lake City, Utah 84112

A total Lagrangian-type nonlinear analysis for prediction of large deformation behavior of thick laminated composite cylindrical shells and panels is presented. The analysis, based on the hypothesis of layerwise linear displacement distribution through thickness, accounts for fully nonlinear kinematic relations, in contrast to the commonly used von Kármán nonlinear strain approximation, so that stable equilibrium paths in the advanced nonlinear regime can be accurately predicted. The resulting degenerated surface-parallel quadratic (16-node) layer element, with 8 nodes on each of the top and bottom surfaces of each layer, has been implemented in conjunction with full and reduced numerical integration schemes to efficiently model both thin and thick shell behavior. The modified Newton–Raphson iterative scheme with Aitken acceleration factors is used to obtain hitherto unavailable numerical results corresponding to fully nonlinear behavior of the analyzed panels. A two-layer [0/90] thin/shallow clamped cylindrical panel is investigated to assess the convergence rate for full and reduced integration schemes and to check the accuracy of the present degenerate cylindrical shell layer element. Accuracy of the von Kármán nonlinear approximation, currently employed in many investigations on buckling/postbuckling behavior of thin shells, is assessed, in the case of laminated thin cylindrical panels, by comparing the numerical results obtained using this approximation with those due to fully nonlinear kinematic relations, especially in the advanced stable postbuckling regime.

Nomenclature

$[A]$ = diagonal matrix composed of Aitken acceleration factors to increase convergence rate
a = half-length of a cylindrical panel
$[B_{LL}]$ = linear differential operator matrix relating the linear incremental strain components to incremental displacement components
$[B_{NL}]$ = linear differential operator matrix relating the linearized incremental strain components to incremental displacement components
$[B_{NN}]$ = linear differential operator matrix relating the nonlinear incremental strain components to incremental displacement components
b, t = subscript or superscript indicating the bottom and the top surface, respectively
C_{ijrs} = elastic stiffness (material property) tensor
$\mathrm{d}S, \mathrm{d}S_0$ = length of line segment on a deformed and an undeformed surface, respectively
${}^0dV$ = infinitesimal control volume with respect to the initial configuration
E_{LT}, E_{TT}, = longitudinal and transverse Young's moduli, respectively
${}_0\bar{e}^L_{ij}$ = linear incremental component of the 6×1 strain vector
${}_0\bar{e}^N_{ij}$ = linearized incremental component of the 6×1 strain vector
$\{f_L\}$ = applied load vector
${}^{t+\Delta t}\{f_L\}$ = applied load vector at time $t + \Delta t$
$\{f_N\}$ = nonlinear internal force vector
${}^{t+\Delta t}\{f_N\}^{(i)}$ = nonlinear internal force vector at the ith iteration of the time step between t and $t + \Delta t$
G_{LT}, G_{TT} = longitudinal and transverse shear moduli, respectively
g_θ = coefficient of the first fundamental differential quadratic form of the surface in the θ direction
h, h_i = thickness of a shell and its ith lamina, respectively
$[K_L]$ = linear global stiffness matrix
$[K_N]$ = nonlinear contribution to the global geometric stiffness matrix
L, T = subscripts indicating the longitudinal and transverse directions, respectively, of a lamina
N = total number of elements
NL = number of elements in each layer
NS = number of layers
$\boldsymbol{n}$ = unit normal vector for the surface with respect to the fixed coordinate system
P_r = applied radial pressure
$[Q], [\bar{Q}]$ = elastic stiffness (material property) matrix for an orthotropic and an anisotropic layer, respectively
$Q^{(k)}_{ij}, \bar{Q}^{(k)}_{ij}$ = stiffness matrix components of the kth orthotropic and anisotropic layer, respectively
$\{{}_0\boldsymbol{Q}\}^{(i)}$ = incremental displacement vector due to the applied load vector
q = uniform radial pressure
$\boldsymbol{R}$ = position vector of an arbitrary point at a distance from the bottom surface of the ith layer
R = mean radius of a cylindrical panel
$\{{}_0\boldsymbol{R}\}^{(i)}$ = incremental displacement vector due to the residual force vector
${}^{t+\Delta t}\Re$ = external virtual work of the body
$\boldsymbol{r}$ = position vector of an arbitrary point on the bottom surface of the ith layer
r, s = natural in-plane coordinates of an isoparametric layer element
${}_0S^{(k)}_{ij}$ = incremental stress component of the kth layer
${}^{t+\Delta t}_0S_{ij}$ = second Piola–Kirchhoff stress tensor at time $t + \Delta t$ evaluated with respect to the initial configuration

Received April 28, 1994; revision received Jan. 25, 1995; accepted for publication Jan. 30, 1995.

*Graduate Research Assistant, Mechanical Engineering Department; currently Structural Analyst, Aircraft Structures Division, Agency for Defense Development, Taejon, Republic of Korea.

†Associate Professor, Civil Engineering Department. Member AIAA.

${}^{t}_{0}\hat{S}_{ij}$ = 9×9 stress matrix evaluated at time t

${}^{t}_{0}\bar{S}_{ij}$ = 6×1 stress vector evaluated at time t

$\left[{}^{t+\Delta t}_{0}\bar{S}^{(k)}\right]^{(i-1)}$ = element stress vector of the kth layer evaluated at $(i-1)$th iteration of each load step.

t = time as an index

${}_0u_b^{(i)}, {}_0v_b^{(i)}, {}_0w_b^{(i)}$ = incremental displacement components at a point on the bottom surface of the ith layer in x^1 (or x), x^2 (or θ), and z directions, respectively

${}_0u_t^{(i)}, {}_0v_t^{(i)}, {}_0w_t^{(i)}$ = incremental displacement components at a point on the top surface of the ith layer in x^1 (or x), x^2 (or θ), and z directions, respectively

${}_0U_{bk}^{(i)}, {}_0V_{bk}^{(i)}, {}_0W_{bk}^{(i)}$ = incremental nodal displacement components at the kth node on the bottom surface of the ith layer in x^1 (or x), x^2 (or θ), and z directions, respectively

${}_0U_{tk}^{(i)}, {}_0V_{tk}^{(i)}, {}_0W_{tk}^{(i)}$ = incremental nodal displacement components at the kth node on the top surface of the ith layer in x_1 (or x), x_2 (or θ), and z directions, respectively

${}^{t+\Delta t}\{V\}^{(i)}$ = total displacement vector at the ith iteration of the time step between t and $t+\Delta t$

${}_0V$ = control volume with respect to the initial configuration

v_i = ith physical component of the displacement vector, $i = 1, 2, 3$

$x^{(i)}, \theta^{(i)}, z^{(i)}$ = coordinates of a point in the element of the ith layer in terms of r and s

α, β, ζ = material coordinates of a fiber-reinforced anisotropic lamina

Γ_{im}^{k} = Christoffel symbol of the second kind

γ_{ij} = Green–Lagrangian strain tensor

ε_{ij} = physical component of Green–Lagrange strain tensor

${}_0\varepsilon_{ij}^{(k)}$ = incremental strain component of the kth layer

${}^{t+\Delta t}_{0}\bar{\varepsilon}_{ij}$ = total Green–Lagrangian strain tensor evaluated on the initial configuration at time $t+\Delta t$

$\hat{\eta}_{ki}, \delta\hat{\eta}_{ki}$ = 9×1 nonlinear strain component vector and its variation, respectively

θ_0 = Half-angular dimension of a cylindrical panel in the circumferential direction

$\rho^{(i)}$ = radius of the bottom surface of the ith layer of a cylindrical shell

$[\Phi]$ = quadratic global interpolation function matrix

ϕ = fiber orientation angle with respect to the x axis

$\psi_k(r, s)$ = quadratic element interpolation function composed in terms of r and s

I. Introduction

THIN cylindrical shells and panels are widely used as structural elements in aerospace, hydrospace, and terrestrial applications. It has been long recognized that collapse/failure behavior of such structural components cannot be well predicted by a linear theory, since it is associated with small displacements and rotations.[1] A nonlinear theory must be incorporated to measure such large displacements and rotations as are often encountered in such components. Analytical solutions are relatively scarce and are primarily restricted to linear analyses and simple geometries. A numerical procedure, such as the finite element method (FEM), appears to be a viable practical alternative because of the ease with which the problems of geometric and material nonlinearities, arbitrary shell geometry, nonuniform thickness, stiffeners and attachments, cutouts, etc., can be handled by this method.

Although a considerable volume of literature exists on linear finite element analysis of laminated shells (see, e.g., Seide and Chaudhuri[2]) and, to some extent, on nonlinear finite element analysis of isotropic shells (see, e.g., Hsia and Chaudhuri[3]), studies pertaining to nonlinear finite element analysis of laminated shells are relatively scarce. Noor and Hartley[4] were possibly the first to present large deformation analysis of laminated shells using mixed isoparametric triangular and quadrilateral elements. Their formulation is based on shallow shell theory that also includes the effect of interlaminar shear deformation. Chang and Sawamiphakdi[5] presented large deformation analysis of laminated shells using "degenerated" three-dimensional isoparametric elements, in which they have utilized the updated Lagrangian (UL) nonlinear formulation. Sarhangnezhad[6] extended the study of Bathe and Bolourchi[7] to the case of laminated shells. Epstein and Glockner[8] assumed a piecewise smooth displacement field to solve nonlinear finite element problems of multilayered shells. Palazzotto and Witt[9] introduced the effect of transverse shear deformation into the formulation to solve nonlinear problems of composite laminates, which guarantee displacement and slope continuity at the laminar interfaces. Extending Sanders' kinematic relations for thin shell theory to incorporate the first-order transverse shear deformation and von Kármán nonlinear strain approximation (KNSA) in the kinematic relations, Reddy and Chandrashekhara[10] solved nonlinear finite element problems of cylindrical and doubly curved laminated panels.

The present study is primarily motivated to predict the large elastic deformation behavior of laminated cylindrically curved panels. The von Kármán nonlinear strain approximation (KNSA) that is expected to overestimate transverse displacements, especially in the advanced nonlinear regime, is usually used to assess the load-carrying capability of an isotropic structure when such a structure shows a stable postbuckling behavior. Whether this discrepancy (overestimation) is worse in the case of thin asymetrically laminated composite structures, analyzed using such an approximation, is not known at this time. A detailed literature search reveals a lack of investigation on the accuracy of the von Kármán nonlinear strain approximation for either isotropic or laminated composite structures such as cylindrically curved panels in the advanced nonlinear regime, which is the primary objective of the present investigation.

The present analysis accounts for all of the nonlinear terms in the kinematic relations, and utilizes the total Lagrangian (TL) formulations in incremental equilibrium equations. A nonlinear degenerated shell layer element is developed to obtain the discretized system equations. A 16-node curvilinear side layer element with 8 nodes on each of the top and bottom surfaces uses assumed quadratic displacement field and is based on the layerwise linear displacement distribution through the laminate thickness (LLDT). The Newton–Raphson iterative scheme with Aitken acceleration factors is used to obtain hitherto unavailable numerical results corresponding to fully nonlinear behavior of the analyzed panels. A two-layer [0/90] thin/shallow clamped cylindrical panel is investigated to assess the convergence rate for full and reduced integration schemes and to check the accuracy of the present degenerate cylindrical shell layer element. Accuracy of the von Kármán nonlinear strain approximation (KNSA), currently employed in many investigations on buckling/postbuckling behavior of thin shells, is assessed, in the case of asymmetrically laminated thin cylindrical panels, by comparing the numerical results obtained using this approximation with those due to fully nonlinear kinematic relations, especially in the advanced stable postbuckling regime.

II. Kinematic Relations of a Shell

General Theory of Elasticity with Finite Strain

Figure 1 shows the schematic of a laminated cylindrical shell (infinitesimal) element. An arbitrary point Q_0 in the ith layer undergoing a displacement $\boldsymbol{u}$ is considered. The Lagrangian coordinate system refers to a particle motion given by $\boldsymbol{X} = \boldsymbol{X}(\boldsymbol{x}, t)$, where $\boldsymbol{x}$ denotes an orthogonal curvilinear coordinate system, defining the position vector of the point Q_0, at time $t = t_0$ in the undeformed state, whereas $\boldsymbol{X}$ denotes the corresponding position vector of the point Q in the deformed state at time t. The difference between the squares of line segments, $(ds)^2$ and $(dS)^2$ on the undeformed and deformed surfaces, respectively, is the measure of strain given by[11]

$$(dS)^2 - (ds)^2 = 2\gamma_{ij}dx_i dx_j \tag{1}$$

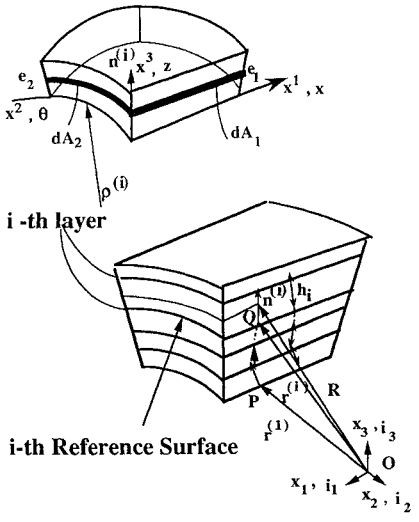

Fig. 1 Geometry of a laminated cylindrical shell (infinitesimal) element.

where γ_{ij} is given by

$$\gamma_{ij} = \tfrac{1}{2}\left(\left[u_{i,j} - u_k\Gamma^k_{ij}\right] + \left[u_{j,i} - u_k\Gamma^k_{ij}\right] + \left[u_{k,i}u^k_{,j} - u_k\Gamma^k_{im}u^m_{,j} + u_{k,i}\Gamma^k_{1j}u^1 - u_k u^1\Gamma^k_{im}\Gamma^m_{1j}\right]\right) \tag{2}$$

in which u_k and u^k are the covariant and contravariant components of the displacement vector, respectively. The physical component v_i of the displacement vector $\boldsymbol{u}$ for an orthogonal coordinate system can be written as (no sum on i)

$$v_i = u_i\sqrt{g^{ii}} = u^i\sqrt{g_{ii}} \tag{3}$$

where g_{ii} and g^{ii} are components of metric and associated metric tensors, respectively. A physical component ε_{ij} of the second-order tensor γ_{ij} can also be obtained as (no sum on i, j)

$$\varepsilon_{ij} = \sqrt{g^{ii}g^{jj}}\gamma_{ij} \tag{4}$$

Substitution of Eqs. (2) and (3) into Eq. (4) yields

$$\varepsilon_{ij} = \frac{1}{2}\sqrt{g^{ii}g^{jj}}\left\{\left[\left(\frac{v_i}{\sqrt{g^{ii}}}\right)_{,j} - \left(\frac{v_k}{\sqrt{g^{kk}}}\right)\Gamma^k_{ij}\right] + \left[\left(\frac{v_j}{\sqrt{g^{jj}}}\right)_{,i} - \left(\frac{v_k}{\sqrt{g^{kk}}}\right)\Gamma^k_{ij}\right] + \left[\left(\frac{v_k}{\sqrt{g^{kk}}}\right)_{,i}\left(\frac{v_k}{\sqrt{g^{kk}}}\right)_{,j} - \left(\frac{v_k}{\sqrt{g^{kk}}}\right)\Gamma^k_{im}\left(\frac{v_m}{\sqrt{g_{mm}}}\right)_{,j} + \left(\frac{v_k}{\sqrt{g^{kk}}}\right)_{,i}\Gamma^k_{1j}\left(\frac{v_1}{\sqrt{g_{11}}}\right) - \left(\frac{v_k}{\sqrt{g^{kk}}}\right)\left(\frac{v_1}{\sqrt{g_{11}}}\right)\Gamma^k_{im}\Gamma^m_{1j}\right]\right\} \tag{5}$$

Nonlinear Kinematic Relations for a Cylindrical Shell layer

Invoking the theory of parallel surfaces, the following relations are obtained for the ith layer of a cylindrical shell[12]:

$$\sqrt{g_{11}} = \sqrt{g_{33}} = 1; \qquad \sqrt{g_{22}} = g^{(i)}_\theta = \rho^{(i)}\left[1 + \frac{z}{\rho^{(i)}}\right] \tag{6}$$

On substituting the physical components of the displacement vector $\boldsymbol{v}$ and the coefficients of the first fundamental differential quadratic form of the surface, given by Eq. (6), into Eq. (5), the components of the engineering nonlinear strain in terms of displacements at an arbitrary point inside the ith layer are obtained as follows (the superscript i is dropped in the remainder of this section and the following one for notational convenience):

$$\varepsilon_{11} = \frac{\partial u}{\partial x} + \frac{1}{2}\left[\left(\frac{\partial u}{\partial x}\right)^2 + \left(\frac{\partial v}{\partial x}\right)^2 + \left(\frac{\partial w}{\partial x}\right)^2\right] \tag{7a}$$

$$\varepsilon_{22} = \frac{1}{g_\theta}\left(\frac{\partial v}{\partial \theta} + w\right) + \frac{1}{2g^2_\theta}\left(\frac{\partial v}{\partial \theta} + w\right)^2 + \frac{1}{2g^2_\theta}\left(\frac{\partial u}{\partial \theta}\right)^2 + \frac{1}{2g^2_\theta}\left(\frac{\partial w}{\partial \theta} - v\right)^2 \tag{7b}$$

$$\varepsilon_{12} = \frac{\partial v}{\partial x} + \frac{1}{g_\theta}\frac{\partial u}{\partial \theta} + \frac{1}{g_\theta}\frac{\partial u}{\partial x}\frac{\partial u}{\partial \theta} + \frac{1}{g_\theta}\left(\frac{\partial v}{\partial \theta} + w\right)\frac{\partial v}{\partial x} + \frac{1}{g_\theta}\left(\frac{\partial w}{\partial \theta} - v\right)\frac{\partial w}{\partial x} \tag{7c}$$

$$\varepsilon_{33} = \frac{\partial w}{\partial z} + \frac{1}{2}\left(\frac{\partial u}{\partial z}\right)^2 + \frac{1}{2}\left(\frac{\partial v}{\partial z}\right)^2 + \frac{1}{2}\left(\frac{\partial w}{\partial z}\right)^2 \tag{7d}$$

$$\varepsilon_{13} = \frac{\partial w}{\partial x} + \frac{\partial u}{\partial z} + \frac{\partial u}{\partial x}\frac{\partial u}{\partial z} + \frac{\partial v}{\partial x}\frac{\partial v}{\partial z} + \frac{\partial w}{\partial x}\frac{\partial w}{\partial z} \tag{7e}$$

$$\varepsilon_{23} = \frac{1}{g_\theta}\left(\frac{\partial w}{\partial \theta} - v\right) + \frac{\partial v}{\partial z} + \frac{1}{g_\theta}\left(\frac{\partial v}{\partial \theta} + w\right)\frac{\partial v}{\partial z} + \frac{1}{g_\theta}\frac{\partial u}{\partial \theta}\frac{\partial u}{\partial z} + \frac{1}{g_\theta}\frac{\partial w}{\partial z}\left(\frac{\partial w}{\partial \theta} - v\right) \tag{7f}$$

where the components of the displacement vector $\boldsymbol{v}$ given by

$$v_1 = u(x^1, x^2, z); \quad v_2 = v(x^1, x^2, z); \quad v_3 = w(x^1, x^2, z) \tag{8}$$

have already been utilized. The von Kármán nonlinear approximation is obtained by setting the nonlinear surface-parallel displacement contributions in Eqs. (7c) and (7d) to zero and keeping only the von Kármán rotation terms in the nonlinear parts of Eq. (7a) and (7b):

$$\varepsilon_{11} = \frac{\partial u}{\partial x} + \frac{1}{2}\left(\frac{\partial w}{\partial x}\right)^2 \tag{9a}$$

$$\varepsilon_{22} = \frac{1}{g_\theta}\left(\frac{\partial v}{\partial \theta} + w\right) + \frac{1}{2g^2_\theta}\left(\frac{\partial w}{\partial \theta}\right)^2 \tag{9b}$$

$$\varepsilon_{12} = \frac{\partial v}{\partial x} + \frac{1}{g_\theta}\frac{\partial u}{\partial \theta} + \frac{1}{g_\theta}\frac{\partial w}{\partial \theta}\frac{\partial w}{\partial x} \tag{9c}$$

$$\varepsilon_{33} = \frac{\partial w}{\partial z} + \frac{1}{2}\left(\frac{\partial w}{\partial z}\right)^2 \tag{9d}$$

$$\varepsilon_{13} = \frac{\partial w}{\partial x} + \frac{\partial u}{\partial z} + \frac{\partial w}{\partial x}\frac{\partial w}{\partial z} \tag{9e}$$

$$\varepsilon_{23} = \frac{1}{g_\theta}\left(\frac{\partial w}{\partial \theta} - v\right) + \frac{\partial v}{\partial z} + \frac{1}{g_\theta}\frac{\partial w}{\partial z}\frac{\partial w}{\partial \theta} \tag{9f}$$

III. Method of Virtual Work—Linearized Equations of Motion

The second Piola–Kirchhoff stress tensor is conjugate to the Green–Lagrange strain tensor in that their properties are also invariant under rigid-body motions. When the equilibrium of the body at time $t + \Delta t$ is first expressed using the principle of virtual displacements with tensor notation, the total Lagrangian formulation requires that

$$\int_{0_V} {}^{t+\Delta t}_{0}S_{ij}\,\delta\,{}^{t+\Delta t}_{0}\bar{\varepsilon}_{ij}\,{}^{0}dV = {}^{t+\Delta t}\Re \tag{10}$$

where

$$ {}^{t+\Delta t}_{0}S_{ij} = {}^{t}_{0}S_{ij} + {}_{0}S_{ij} \tag{11} $$

$$ {}^{t+\Delta t}_{0}\bar{\varepsilon}_{ij} = {}^{t}_{0}\bar{\varepsilon}_{ij} + {}_{0}\bar{\varepsilon}_{ij}; \qquad {}_{0}\bar{\varepsilon}_{ij} = {}_{0}\bar{e}_{ij} + {}_{0}\bar{\eta}_{ij} \tag{12} $$

The quantities ${}_{0}\bar{e}_{ij}$ and ${}_{0}\bar{\eta}_{ij}$ in Eq. (12) denote the linear and the nonlinear incremental strains, respectively, that are referred to the initial configuration. The linear strain vector $\{{}_{0}\bar{e}_{ij}\}$ is here resolved into two parts that are the purely linear part, $\{{}_{0}\bar{e}^{L}_{ij}\}$ and the linearized part, $\{{}_{0}\bar{e}^{N}_{ij}\}$. Substituting Eq. (11) and (12) and the constitutive relations

$$ {}_{0}S_{ij} = C_{ijrs}\,{}_{0}\bar{\varepsilon}_{rs} \tag{13} $$

into the left-hand side of Eq. (10) finally yields the following:

$$ \begin{aligned} &\int_{0_V} \left({}^{t}_{0}S_{ij} + {}_{0}S_{ij}\right)\delta\left({}^{t}_{0}\bar{\varepsilon}_{ij} + {}_{0}\bar{\varepsilon}_{ij}\right){}^{0}dV \\ &\cong \int_{0_V} C_{ijrs}\,{}_{0}\bar{e}^{L}_{rs}\,\delta_{0}\bar{e}^{L}_{ij}\,{}^{0}dV + \int_{0_V} C_{ijrs}\,{}_{0}\bar{e}^{N}_{rs}\,\delta_{0}\bar{e}^{L}_{ij}\,{}^{0}dV \\ &+ \int_{0_V} C_{ijrs}\,{}_{0}\bar{e}^{L}_{rs}\,\delta_{0}\bar{e}^{N}_{ij}\,{}^{0}dV + \int_{0_V} C_{ijrs}\,{}_{0}\bar{e}^{N}_{rs}\,\delta_{0}\bar{e}^{N}_{ij}\,{}^{0}dV \\ &+ \int_{0_V} \delta\hat{\eta}_{ki}\,{}^{t}_{0}\hat{S}_{ij}\,\hat{\eta}_{kj}\,{}^{0}dV + \int_{0_V} {}^{t}_{0}\bar{S}_{ij}\left\{\delta_{0}\bar{e}^{L}_{ij} + \delta_{0}\bar{e}^{N}_{ij}\right\}{}^{0}dV \end{aligned} \tag{14} $$

in which terms of degree 2 or higher in this equation are so small, compared with other terms, that those terms can be neglected. The constitutive relation for the ith lamina, referred to the material coordinates at the initial configuration ($\alpha = x$, $\beta = \theta$, $\zeta = z$), can be written as follows:

$$ \begin{Bmatrix} {}_{0}S^{(i)}_{\alpha\alpha} \\ {}_{0}S^{(i)}_{\beta\beta} \\ {}_{0}S^{(i)}_{\zeta\zeta} \\ {}_{0}S^{(i)}_{\beta\zeta} \\ {}_{0}S^{(i)}_{\alpha\zeta} \\ {}_{0}S^{(i)}_{\alpha\beta} \end{Bmatrix} = \begin{bmatrix} Q_{11} & Q_{12} & Q_{13} & 0 & 0 & 0 \\ Q_{12} & Q_{22} & Q_{23} & 0 & 0 & 0 \\ Q_{13} & Q_{23} & Q_{33} & 0 & 0 & 0 \\ 0 & 0 & 0 & Q_{44} & 0 & 0 \\ 0 & 0 & 0 & 0 & Q_{55} & 0 \\ 0 & 0 & 0 & 0 & 0 & Q_{66} \end{bmatrix} \begin{Bmatrix} {}_{0}\varepsilon^{(i)}_{\alpha\alpha} \\ {}_{0}\varepsilon^{(i)}_{\beta\beta} \\ {}_{0}\varepsilon^{(i)}_{\zeta\zeta} \\ {}_{0}\varepsilon^{(i)}_{\beta\zeta} \\ {}_{0}\varepsilon^{(i)}_{\alpha\zeta} \\ {}_{0}\varepsilon^{(i)}_{\alpha\beta} \end{Bmatrix} \tag{15} $$

The corresponding constitutive relation for an anisotropic lamina can be obtained using the standard tensor transformation rule.

Using Eq. (7) and (12), one can represent each strain component in Eq.(14) in the matrix form as follows:

$$ \left\{{}_{0}\bar{e}^{L}\right\} = [\boldsymbol{B}_{LL}]\{{}_{0}v\} \tag{16a} $$

$$ \left\{{}_{0}\bar{e}^{N}\right\} = [\boldsymbol{B}_{NL}]\{{}_{0}v\} \tag{16b} $$

$$ \{{}_{0}\hat{\eta}\} = [\boldsymbol{B}_{NN}]\{{}_{0}v\} \tag{16c} $$

where

$$ \{{}_{0}v\} = \left\{{}_{0}u \quad {}_{0}v \quad {}_{0}w\right\}^{T} \tag{17a} $$

$$ \left\{{}_{0}\bar{e}^{L}\right\} = \left\{{}_{0}\bar{e}^{L}_{xx} \quad {}_{0}\bar{e}^{L}_{\theta\theta} \quad {}_{0}\bar{e}^{L}_{zz} \quad {}_{0}\bar{e}^{L}_{z\theta} \quad {}_{0}\bar{e}^{L}_{xz} \quad {}_{0}\bar{e}^{L}_{x\theta}\right\}^{T} \tag{17b} $$

$$ \left\{{}_{0}\bar{e}^{N}\right\} = \left\{{}_{0}\bar{e}^{N}_{xx} \quad {}_{0}\bar{e}^{N}_{\theta\theta} \quad {}_{0}\bar{e}^{N}_{zz} \quad {}_{0}\bar{e}^{N}_{z\theta} \quad {}_{0}\bar{e}^{N}_{xz} \quad {}_{0}\bar{e}^{N}_{x\theta}\right\}^{T} \tag{17c} $$

$$ \{{}_{0}\hat{\eta}\} = \{{}_{0}\hat{\eta}_{xx} \quad {}_{0}\hat{\eta}_{x\theta} \quad {}_{0}\hat{\eta}_{xz} \quad {}_{0}\hat{\eta}_{\theta x} \quad {}_{0}\hat{\eta}_{\theta\theta} \quad {}_{0}\hat{\eta}_{\theta z} \quad {}_{0}\hat{\eta}_{zx} \quad {}_{0}\hat{\eta}_{z\theta} \quad {}_{0}\hat{\eta}_{zz}\}^{T} \tag{17d} $$

The differential operators $[\boldsymbol{B}_{LL}]$, $[\boldsymbol{B}_{NL}]$, and $[\boldsymbol{B}_{NN}]$ are as presented in Eq. (A1), (A2), (A3a–A3c), and (A7), respectively, in the Appendix.

Because the variation in the strain components is equivalent to the use of virtual strains, the right-hand side of Eq. (10) is the virtual work done by the applied loading when the body is subjected to a virtual displacement at time $t + \Delta t$. When the constant directional (dead) pressure is applied, the loading is deformation independent and the external virtual work can be evaluated using the initial configuration as follows:

$$ {}^{t+\Delta t}\Re = \int_{0_S} {}^{t+\Delta t}_{0}f^{S}_{i}\,\delta v^{S0}_{i}\,dS \tag{18} $$

where the ${}^{t+\Delta t}_{0}f^{S}_{i}$ is the surface force vector applied on the surface S at time $t + \Delta t$, and $\delta_{0}v^{S}_{i}$ is the ith component of the incremental virtual displacement vector evaluated on the loaded surface.

IV. Isoparametric Finite Element Discretization for Cylindrical Geometry

In this section, a general nonlinear displacement-based finite element formulation for cylindrical geometry is presented. The basic steps in the derivation of finite element equations are to select the interpolation functions of the displacements and the element coordinates. Because the new element coordinates are obtained by adding the element displacements to the original coordinates in the incremental analysis, the same interpolations can be employed for the displacements and coordinates. In the present study, 16-node quadrilateral layer elements (Fig. 2) are employed because of their computational efficiency, as compared with their lower order linear counterparts, which are too stiff to model the shear deformation of each lamina in the laminate.

The convected coordinates of a generic point (x, θ, z) in an element of the ith layer with eight nodal points on each of the top and bottom surfaces are, in terms of the natural coordinates r and s, given by

$$ \begin{aligned} x^{(i)}(r,s,z) &= \left(1 - \frac{z}{h_i}\right)\sum_{k=1}^{8}\psi_k(r,s)\,{}_{b}x^{(i)}_{k} \\ &+ \frac{z}{h_i}\sum_{k=1}^{8}\psi_k(r,s)\,{}_{t}x^{(i)}_{k} \end{aligned} \tag{19a} $$

$$ \begin{aligned} \theta^{(i)}(r,s,z) &= \left(1 - \frac{z}{h_i}\right)\sum_{k=1}^{8}\psi_k(r,s)\,{}_{b}\theta^{(i)}_{k} \\ &+ \frac{z}{h_i}\sum_{k=1}^{8}\psi_k(r,s)\,{}_{t}\theta^{(i)}_{k} \end{aligned} \tag{19b} $$

$$ \begin{aligned} z^{(i)}(r,s,z) &= \left(1 - \frac{z}{h_i}\right)\sum_{k=1}^{8}\psi_k(r,s)\,{}_{b}z^{(i)}_{k} \\ &+ \frac{z}{h_i}\sum_{k=1}^{8}\psi_k(r,s)\,{}_{t}z^{(i)}_{k} \end{aligned} \tag{19c} $$

where $\psi_k(r,s)$ represents the interpolation functions taking a value of unity at node k and zero at all other nodes.[13] The quantities ${}_{b}x^{(i)}_{k}$, ${}_{b}\theta^{(i)}_{k}$, ${}_{b}z^{(i)}_{k}$ and ${}_{t}x^{(i)}_{k}$, ${}_{t}\theta^{(i)}_{k}$, ${}_{t}z^{(i)}_{k}$ are coordinates of the nodal point k on the bottom and top surfaces of the ith layer, respectively. In the layerwise linear displacement theory, the incremental displacements of the ith lamina are given by

$$ \left\{{}_{0}v^{(i)}\right\} = \left[\boldsymbol{T}^{(i)}_{BT}(z)\right][\Phi(r,s)]\left\{{}_{0}\boldsymbol{V}^{(i)}_{BT}\right\} \tag{20} $$

in which $[\boldsymbol{T}^{(i)}_{BT}]$ is the linear matrix operator for the ith layer

$$ \left[\boldsymbol{T}^{(i)}_{BT}(z)\right] = \begin{bmatrix} 1 - \frac{z}{h_i} & 0 & 0 & \frac{z}{h_i} & 0 & 0 \\ 0 & 1 - \frac{z}{h_i} & 0 & 0 & \frac{z}{h_i} & 0 \\ 0 & 0 & 1 - \frac{z}{h_i} & 0 & 0 & \frac{z}{h_i} \end{bmatrix} \tag{21a} $$

whereas the nodal displacement vector $\{{}_{0}\boldsymbol{V}^{(i)}_{BT}\}$ of the ith layer is defined by

$$ \begin{aligned} \left\{{}_{0}\boldsymbol{V}^{(i)}_{BT}\right\}^{T} &= \left\{{}_{0}U^{(i)}_{b1} \bullet\bullet {}_{0}U^{(i)}_{b8}\ {}_{0}V^{(i)}_{b1} \bullet\bullet {}_{0}V^{(i)}_{b8}\ {}_{0}W^{(i)}_{b1} \bullet\bullet {}_{0}W^{(i)}_{b8}\right. \\ &\times {}_{0}U^{(i)}_{t1} \bullet\bullet {}_{0}U^{(i)}_{t8}\ {}_{0}V^{(i)}_{t1} \bullet\bullet {}_{0}V^{(i)}_{t8}\ {}_{0}W^{(i)}_{t1} \bullet\bullet {}_{0}W^{(i)}_{t8}\Big\} \end{aligned} \tag{21b} $$

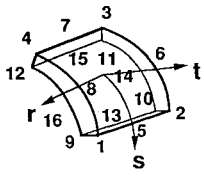

Fig. 2 16-node curvilinear side surface-parallel quadratic isoparametric element.

and

$$[\Phi(r,s)] = \begin{bmatrix} \{\psi\} & \{0\} & \{0\} & \{0\} & \{0\} & \{0\} \\ \{0\} & \{\psi\} & \{0\} & \{0\} & \{0\} & \{0\} \\ \{0\} & \{0\} & \{\psi\} & \{0\} & \{0\} & \{0\} \\ \{0\} & \{0\} & \{0\} & \{\psi\} & \{0\} & \{0\} \\ \{0\} & \{0\} & \{0\} & \{0\} & \{\psi\} & \{0\} \\ \{0\} & \{0\} & \{0\} & \{0\} & \{0\} & \{\psi\} \end{bmatrix} \tag{21c}$$

wherein $\{\psi\} = \{\psi_1\ \psi_2\ \psi_3\ \psi_4\ \psi_5\ \psi_6\ \psi_7\ \psi_8\}$ and $\{0\}$ is 1×8 null matrix. Ther term $\psi_k(r,s)$, $k = 1, \ldots, 8$, represents the same interpolation functions used in Eq. (19).

The right-hand side of Eq. (14) can here be rewritten using the matrix differential operators, $\boldsymbol{B}_{LL}$, $\boldsymbol{B}_{LN}$, $\boldsymbol{B}_{NN}$, and $\boldsymbol{T}_{BT}^{(i)}$ defined in the Eqs. (16), (17), and (21), as follows:

$$\begin{aligned}
&\int_{0V} C_{ijrs0}\bar{e}_{rs}^{L}\delta_0\bar{e}_{ij}^{L0}dV + \int_{0V} C_{ijrs0}\bar{e}_{rs}^{N}\delta_0\bar{e}_{ij}^{L0}dV \\
&+ \int_{0V} C_{ijrs0}\bar{e}_{rs}^{L}\delta_0\bar{e}_{ij}^{N0}dV + \int_{0V} C_{ijrs0}\bar{e}_{rs}^{N}\delta_0\bar{e}_{ij}^{N0}dV \\
&+ \int_{0V} \delta\hat{\eta}_{ki}{}_0^t\hat{S}_{ij}\hat{\eta}_{kj}{}^0dV + \int_{0V} {}_0^t\bar{S}_{ij}\left\{\delta_0\bar{e}_{ij}^{L} + \delta_0\bar{e}_{ij}^{N}\right\}^0dV \\
&= \int_{0S}\sum_{k=1}^{NS}\int_{h_{k-1}}^{h_k} \delta\left\{{}_0\boldsymbol{V}_{BT}^{(k)}\right\}^T\left(\left[\boldsymbol{B}_{LL}^{(k)}\right]\left[\boldsymbol{T}_{BT}^{(k)}\right][\Phi]\right)^T\left[\bar{Q}^{(k)}\right] \\
&\times\left[\boldsymbol{B}_{LL}^{(k)}\right]\left[\boldsymbol{T}_{BT}^{(k)}\right][\Phi]\left\{{}_0\boldsymbol{V}_{BT}^{(k)}\right\}\rho^{(k)}\,\mathrm{d}z\,\mathrm{d}\theta\,\mathrm{d}x \\
&+ \int_{0S}\sum_{k=1}^{NS}\int_{h_{k-1}}^{h_k} \delta\left\{{}_0\boldsymbol{V}_{BT}^{(k)}\right\}^T\left(\left[\boldsymbol{B}_{NL}^{(k)}\right]\left[\boldsymbol{T}_{BT}^{(k)}\right][\Phi]\right)^T\left[\bar{Q}^{(k)}\right] \\
&\times\left[\boldsymbol{B}_{LL}^{(k)}\right]\left[\boldsymbol{T}_{BT}^{(k)}\right][\Phi]\left\{{}_0\boldsymbol{V}_{BT}^{(k)}\right\}\rho^{(k)}\,\mathrm{d}z\,\mathrm{d}\theta\,\mathrm{d}x \\
&+ \int_{0S}\sum_{k=1}^{NS}\int_{h_{k-1}}^{h_k} \delta\left\{{}_0\boldsymbol{V}_{BT}^{(k)}\right\}^T\left(\left[\boldsymbol{B}_{LL}^{(k)}\right]\left[\boldsymbol{T}_{BT}^{(k)}\right][\Phi]\right)^T\left[\bar{Q}^{(k)}\right] \\
&\times\left[\boldsymbol{B}_{NL}^{(k)}\right]\left[\boldsymbol{T}_{BT}^{(k)}\right][\Phi]\left\{{}_0\boldsymbol{V}_{BT}^{(k)}\right\}\rho^{(k)}\,\mathrm{d}z\,\mathrm{d}\theta\,\mathrm{d}x \\
&+ \int_{0S}\sum_{k=1}^{NS}\int_{h_{k-1}}^{h_k} \delta\left\{{}_0\boldsymbol{V}_{BT}^{(k)}\right\}^T\left(\left[\boldsymbol{B}_{NL}^{(k)}\right]\left[\boldsymbol{T}_{BT}^{(k)}\right][\Phi]\right)^T\left[\bar{Q}^{(k)}\right] \\
&\times\left[\boldsymbol{B}_{NL}^{(k)}\right]\left[\boldsymbol{T}_{BT}^{(k)}\right][\Phi]\left\{{}_0\boldsymbol{V}_{BT}^{(k)}\right\}\rho^{(k)}\,\mathrm{d}z\,\mathrm{d}\theta\,\mathrm{d}x \\
&+ \int_{0S}\sum_{k=1}^{NS}\int_{h_{k-1}}^{h_k} \delta\left\{{}_0\boldsymbol{V}_{BT}^{(k)}\right\}^T\left(\left[\boldsymbol{B}_{NN}^{(k)}\right]\left[\boldsymbol{T}_{BT}^{(k)}\right][\Phi]\right)^T\left[{}_0^t\hat{S}^{(k)}\right] \\
&\times\left[\boldsymbol{B}_{NN}^{(k)}\right]\left[\boldsymbol{T}_{BT}^{(k)}\right][\Phi]\left\{{}_0\boldsymbol{V}_{BT}^{(k)}\right\}\rho^{(k)}\,\mathrm{d}z\,\mathrm{d}\theta\,\mathrm{d}x \\
&+ \int_{0S}\sum_{k=1}^{NS}\int_{h_{k-1}}^{h_k} \delta\left\{{}_0\boldsymbol{V}_{BT}^{(k)}\right\}^T\left(\left[\boldsymbol{B}_{LL}^{(k)}\right]\left[\boldsymbol{T}_{BT}^{(k)}\right][\Phi]\right)^T \\
&\times\left[{}_0^t\bar{S}^{(k)}\right]\rho^{(k)}\,\mathrm{d}z\,\mathrm{d}\theta\,\mathrm{d}x \\
&+ \int_{0S}\sum_{k=1}^{NS}\int_{h_{k-1}}^{h_k} \delta\left\{{}_0\boldsymbol{V}_{BT}^{(k)}\right\}^T\left(\left[\boldsymbol{B}_{NL}^{(k)}\right]\left[\boldsymbol{T}_{BT}^{(k)}\right][\Phi]\right)^T \\
&\times\left[{}_0^t\bar{S}^{(k)}\right]\rho^{(k)}\,\mathrm{d}z\,\mathrm{d}\theta\,\mathrm{d}x
\end{aligned} \tag{22}$$

in which

$$\left[{}_0^t\hat{S}_{ij}\right] = \begin{bmatrix} \left[{}_0^tS'\right] & [0] & [0] \\ [0] & \left[{}_0^tS'\right] & [0] \\ [0] & [0] & \left[{}_0^tS'\right] \end{bmatrix} \tag{23}$$

with

$$\left[{}_0^tS'\right] = \begin{bmatrix} {}_0^tS_{xx} & {}_0^tS_{x\theta} & {}_0^tS_{x\zeta} \\ {}_0^tS_{x\theta} & {}_0^tS_{\theta\theta} & {}_0^tS_{\zeta\theta} \\ {}_0^tS_{x\zeta} & {}_0^tS_{\theta\zeta} & {}_0^tS_{\zeta\zeta} \end{bmatrix} \tag{24}$$

and

$$\left\{{}_0^t\bar{S}_{ij}\right\} = \left\{{}_0^tS_{xx}\quad {}_0^tS_{\theta\theta}\quad {}_0^tS_{\zeta\zeta}\quad {}_0^tS_{\theta\zeta}\quad {}_0^tS_{x\zeta}\quad {}_0^tS_{x\theta}\right\} \tag{25}$$

Similar operations on Eq. (18) yield the following:

$$\begin{aligned}
&\int_{t+\Delta t_{S^{(k-1)}}} {}_0^{t+\Delta t}f_i^S\delta_0v_i^{St+\Delta t}\,\mathrm{d}S \\
&= \int_S \delta\left\{{}_0\boldsymbol{V}_{BT}^{(NS)}\right\}^T\left(\left[\boldsymbol{T}_{BT}^{(NS)}(h)\right][\Phi]\right)^T\{\boldsymbol{n}^{(NS+1)}\}P_r\rho^{(NS)}\,\mathrm{d}x\,\mathrm{d}\theta
\end{aligned} \tag{26}$$

On computing the right-hand sides of Eqs. (22) and (26) as sums of integrations over the volumes and areas of all finite elements, followed by equating them, and incorporating the boundary conditions, the principle of virtual displacement is invoked to obtain the incremental equations of motion as follows:

$$[\boldsymbol{K}_L]\{{}_0\boldsymbol{V}\} + [\boldsymbol{K}_N]\{{}_0\boldsymbol{V}\} = \{f_L\} - \{f_N\} \tag{27}$$

where

$$\begin{aligned}
[\boldsymbol{K}_L] \equiv &\sum_{m=1}^{NL}\sum_{k=1}^{NS}\int_{S^{(m)}}\int_{h_{k-1}}^{h_k}\left(\left[\boldsymbol{B}_{LL}^{(k)}\left[\boldsymbol{T}_{BT}^{(k)}\right]\right][\Phi]\right)^T\left[\bar{Q}^{(k)}\right] \\
&\times\left[\boldsymbol{B}_{LL}^{(k)}\right]\left[\boldsymbol{T}_{BT}^{(k)}\right][\Phi]\rho^{(k)}\,\mathrm{d}z\,\mathrm{d}S
\end{aligned} \tag{28a}$$

$$\begin{aligned}
[\boldsymbol{K}_N] \equiv &\sum_{m=1}^{NL}\sum_{k=1}^{NS}\int_{S^{(m)}}\int_{h_{k-1}}^{h_k} 2\left(\left[\boldsymbol{B}_{LL}^{(k)}\left[\boldsymbol{T}_{BT}^{(k)}\right]\right][\Phi]\right)^T\left[\bar{Q}^{(k)}\right] \\
&\times\left[\boldsymbol{B}_{NL}^{(k)}\right]\left[\boldsymbol{T}_{BT}^{(k)}\right][\Phi]\rho^{(k)}\,\mathrm{d}z\,\mathrm{d}S \\
&+\sum_{m=1}^{NL}\sum_{k=1}^{NS}\int_{S^{(m)}}\int_{h_{k-1}}^{h_k}\left(\left[\boldsymbol{B}_{NL}^{(k)}\left[\boldsymbol{T}_{BT}^{(k)}\right][\Phi]\right)^T\left[\bar{Q}^{(k)}\right]\right. \\
&\times\left[\boldsymbol{B}_{NL}^{(k)}\right]\left[\boldsymbol{T}_{BT}^{(k)}\right][\Phi]\rho^{(k)}\,\mathrm{d}z\,\mathrm{d}S \\
&+\sum_{m=1}^{NL}\sum_{k=1}^{NS}\int_{S^{(m)}}\int_{h_{k-1}}^{h_k}\left(\left[\boldsymbol{B}_{NN}^{(k)}\right]\left[\boldsymbol{T}_{BT}^{(k)}\right][\Phi]\right)^T\left[{}_0^t\hat{S}^{(k)}\right] \\
&\times\left[\boldsymbol{B}_{NN}^{(k)}\right]\left[\boldsymbol{T}_{BT}^{(k)}\right][\Phi]\rho^{(k)}\,\mathrm{d}z\,\mathrm{d}S
\end{aligned} \tag{28b}$$

$$\{f_L\} \equiv \sum_{m=1}^{N}\int_{S^{(m)}}\left[\left[\boldsymbol{T}_{BT}^{(NS)}\right][\Phi]\right]^T\left\{n^{(NS+1)}\right\}P_r\rho^{(NS)}\,\mathrm{d}S \tag{29a}$$

$$\begin{aligned}
\{f_N\} \equiv &\sum_{m=1}^{NL}\sum_{k=1}^{NS}\int_{S^{(m)}}\int_{h_{k-1}}^{h_k}\left(\left[\boldsymbol{B}_{LL}^{(k)}\right]\left[\boldsymbol{T}_{BT}^{(k)}\right][\Phi]\right)^T\left[{}_0^t\bar{S}^{(k)}\right]\rho^{(k)}\,\mathrm{d}z\,\mathrm{d}S \\
&+\sum_{m=1}^{NL}\sum_{k=1}^{NS}\int_{S^{(m)}}\int_{h_{k-1}}^{h_k}\left(\left[\boldsymbol{B}_{NL}^{(k)}\right]\left[\boldsymbol{T}_{BT}^{(k)}\right][\Phi]\right)^T\left[{}_0^t\bar{S}^{(k)}\right]\rho^{(k)}\,\mathrm{d}z\,\mathrm{d}S
\end{aligned} \tag{29b}$$

and

$$
\begin{aligned}
&\{{}_0V\}^T \\
&= \{{}_0U_{b1}^{(1)} \bullet\bullet {}_0U_{b8}^{(1)}\ {}_0V_{b1}^{(1)} \bullet\bullet {}_0V_{b8}^{(1)}\ {}_0W_{b1}^{(1)} \bullet\bullet {}_0W_{b8}^{(1)} \\
&\times {}_0U_{t1}^{(1)} \bullet\bullet {}_0U_{t8}^{(1)}\ {}_0V_{t1}^{(1)} \bullet\bullet {}_0V_{t8}^{(1)}\ {}_0W_{t1}^{(1)} \bullet\bullet {}_0W_{t8}^{(1)} \\
&\times {}_0U_{b1}^{(i)} \bullet\bullet {}_0U_{b8}^{(i)}\ {}_0V_{b1}^{(i)} \bullet\bullet {}_0V_{b8}^{(i)}\ {}_0W_{b1}^{(i)} \bullet\bullet {}_0W_{b8}^{(i)} \\
&\times {}_0U_{t1}^{(i)} \bullet\bullet {}_0U_{t8}^{(i)}\ {}_0V_{t1}^{(i)} \bullet\bullet {}_0V_{t8}^{(i)}\ {}_0W_{t1}^{(i)} \bullet\bullet {}_0W_{t8}^{(i)} \\
&\times {}_0U_{b1}^{(N)} \bullet\bullet {}_0U_{b8}^{(N)}\ {}_0V_{b1}^{(N)} \bullet\bullet {}_0V_{b8}^{(N)}\ {}_0W_{b1}^{(N)} \bullet\bullet {}_0W_{b8}^{(N)} \\
&\times {}_0U_{t1}^{(N)} \bullet\bullet {}_0U_{t8}^{(N)}\ {}_0V_{t1}^{(N)} \bullet\bullet {}_0V_{t8}^{(N)}\ {}_0W_{t1}^{(N)} \bullet\bullet {}_0W_{t8}^{(N)}\} \qquad (30)
\end{aligned}
$$

Note that total number of elements N equals NL^*NS.

V. Iterative Solution Strategy

Because the nodal point forces at time $t + \Delta t$ depend nonlinearly on the nodal point displacements, it is necessary to iterate for obtaining a reasonably accurate solution of Eq. (27). The most frequently used iteration scheme for solutions of nonlinear finite element equations is the Newton–Raphson iteration because reformations and triangularizations of stiffness matrices at selective load and iteration steps are considered computationally more efficient. In the modified Newton–Raphson method, only the stress force vector [see Eq. (27)] is modified without changing the stiffness matrix after each iteration of a certain load step and the following algorithm for Eq. (27) is developed:

$$
\big([K_L] + {}^t[K_N]\big)\{{}_0V\}^{(i)} = {}^{t+\Delta t}\{f_L\} - {}^{t+\Delta t}\{f_N\}^{(i-1)} \qquad (31)
$$

$$
{}^{t+\Delta t}\{V\}^{(i)} = {}^{t+\Delta t}\{V\}^{(i-1)} + [A]^{(i)}\{{}_0V\}^{(i)} \qquad (32)
$$

with the initial conditions ${}^{t+\Delta t}\{f_N\}^{(0)} = {}^t\{f_N\}$ and ${}^{t+\Delta t}\{V\}^{(0)} = {}^t\{V\}$, where the index i means the number of iterations performed in a certain time step between t and $t + \Delta t$; the subscripts L and N denote the linear and the nonlinear components evaluated at the time t. Equation (31) is equivalent to Eq. (27). Furthermore, in the computer program, the process of the assemblage for the total stiffness matrix can be divided into two groups: the first group is composed of linear elements, where stiffness matrices of each individual element are only calculated at the first load step and remain unchanged during whole loading process. The second one refers to the nonlinear elements where nonlinear stiffness matrices of the element can be evaluated at the first iteration of each load step with nonlinear force vectors, at each iteration of every load step using the contributions of current displacements or stresses. It may be noted here that normal direction vectors and differential area of the loaded surface reduce to their respective constant values evaluated at the first iteration of the first load step when the constant directional load is applied. The 6×1 element stress vector $\{{}^{t+\Delta t}{}_0\bar{S}^{(k)}\}^{(i-1)}$ can be calculated by generalizing the linear elastic relations, $\{{}^{t+\Delta t}{}_0\bar{S}^{(k)}\}^{(i-1)} = [{}^t_0\bar{Q}^{(k)}]^{(i-1)}\{{}^{t+\Delta t}_0\bar{\varepsilon}^{(k)}\}^{(i-1)}$ (Hooke's law in infinitesimal displacement conditions) for the linear material because the second Piola–Kirchhoff stress and Green–Lagrangian strain tensors are invariant under rigid-body motions in large displacement and rotation. The same procedure can be applied to evaluate the 9×9 element stress matrix $[{}^t_0\hat{S}^{(k)}]$ that appears in the nonlinear stiffness matrix of Eq. (28b).

In actual computer programming, the active columns and the addresses of the diagonal elements of the total stiffness matrix are stored effectively in a one-dimensional array and an effective subroutine COLSOL (active column solver) is used to finally obtain the incremental displacement for the unbalanced force, ${}^{t+\Delta t}\Delta R^{(i-1)} = {}^{t+\Delta t}\{f_L\} - {}^{t+\Delta t}\{f_N\}^{(i-1)}$ in the $(i-1)$th iteration. The iteration is continued until the out-of-balance load vector and the displacement increments are sufficiently small; i.e., the iteration scheme is terminated at the current load step and moves to the next load step, when the force convergence criterion,

$$
\frac{\left\|{}^{t+\Delta t}\{f_L\} - {}^{t+\Delta t}\{f_N\}^{(i)}\right\|}{\left\|{}^{t+\Delta t}\{f_L\} - {}^t\{f_L\}\right\|} < \varepsilon_f \qquad (33a)
$$

and the energy convergence criterion,

$$
\frac{\{{}_0V\}^{(i)T}\left[{}^{t+\Delta t}\{f_L\} - {}^{t+\Delta t}\{f_N\}^{(i-1)}\right]}{\{{}_0V\}^{(1)T}\left[{}^{t+\Delta t}\{f_L\} - {}^t\{f_L\}\right]} < \varepsilon_e \qquad (33b)
$$

are simultaneously satisfied, where ε_f and ε_e are preset force and energy tolerances and $\|\cdot\|$ denotes the Euclidean norm of the column vector. The Newton–Raphson method with large value of load increment requires a number of iterations in the nonlinear regime; it may introduce serious errors and, indeed, diverge from the exact solution. Therefore, a rather small load increment would be necessary in the nonlinear regime. It may, however, be noted that the larger value of load increment is recommended with a certain accuracy, for the linear regime, in the interest of computational efficiency.

VI. Numerical Results and Discussion

For our example we analyze a clamped cylindrically curved thin panel under uniform loading.

A two-layer cross-ply [0/90] cylindrical panel of uniform thickness (Fig. 3) is investigated for the purpose of comparison of the present results with those due to Reddy and Chandrashekhara.[10] The geometric and material property data are listed in Table 1. The panel is rigidly clamped so that all of the displacement components, u, v, and w, vanish at the edges of the panel (C2 boundary conditions). Double symmetry conditions permit the model under consideration to be limited to only a quarter of the geometry such that the corresponding surface-parallel displacements vanish along the centerlines and the buckled shapes are assumed to be symmetric. In this study, the surface aspect ratio of each shell-layer element is kept close to 1, for numerical reasons, to ensure uniform convergence of displacement.[14]

First, a convergence study of the present quadrilateral 16-node layer element employed in this example is shown in Fig. 4. Numerical results for a cross-ply [0/90] cylindrical panel are obtained for transverse displacement (deflection), w, at the center of the panel using different number of elements and selective load increments. The pressure load is varied well into the nonlinear regime. The results shown in Fig. 5 and Table 2 reveal that the displacements converge reasonably rapidly for 7×7 mesh with the full integration scheme (FIS): $3 \times 3 \times 2$ Gaussian integration points[15]). It may be noted from Fig. 6 that the reduced integration scheme (RIS): $(2 \times 2 \times 2$ Gaussian integration points) with 4×4 mesh gives almost the same accuracy as that obtained with 7×7 mesh using the full integration scheme.

Table 1 Geometric and material property data of a cross-ply [0/90] cylindrical panel

Geometry	Material property
$R = 2540$ in.	$E_{LL} = 25.00$ Msi
$a = 254$ in.	$E_{TT} = 1.00$ Msi
$h = 2.54$ in.	$G_{LT} = 0.50$ Msi
$\theta_0 = 0.1$ rad	$G_{TT} = 0.20$ Msi
	$\nu_{LT} = 0.25$

Material data with respect to the global coordinate (x, θ, z) for different layup

Layup	E_{xx}	$E_{\theta\theta}$	E_{zz}	$G_{x\theta}$	G_{xz}	$G_{\theta z}$
$\phi = 0$	E_{LL}	E_{TT}	E_{TT}	G_{LT}	G_{LT}	G_{TT}
$\phi = 90$	E_{TT}	E_{LL}	E_{TT}	G_{LT}	G_{TT}	G_{LT}

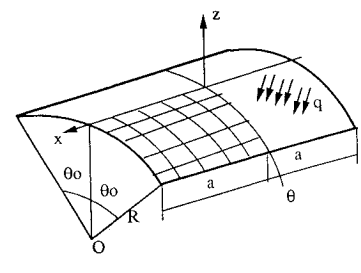

Fig. 3 Geometric modeling of a clamped cross-ply [0/90] cylindrical panel under uniformly distributed loading.

Table 2 Convergence of central (max.) deflection of a clamped cross-ply [0/90] cylindrical panel at different load steps

Load, psi	Deflection, in.						
	4 × 4 mesh		6 × 6 mesh		7 × 7 mesh	8 × 8 mesh	10 × 10 mesh
	FIS	RIS	FIS	RIS	FIS	FIS	FIS
0.00	0.00000	0.00000	0.00000	0.00000	0.00000	0.00000	0.00000
0.10	−0.03737	−0.03690	−0.03743	−0.03736	−0.03754	−0.03749	−0.03724
0.20	−0.07610	−0.07517	−0.07618	−0.07609	−0.07641	−0.07632	−0.07585
0.30	−0.11607	−0.11509	−0.11653	−0.11652	−0.11691	−0.11680	−0.11614
0.40	−0.15764	−0.15709	−0.15885	−0.15908	−0.15941	−0.15932	−0.15853
0.50	−0.20113	−0.20178	−0.20366	−0.20440	−0.20447	−0.20446	−0.20364
0.60	−0.24698	−0.25006	−0.25172	−0.25344	−0.25290	−0.25308	−0.25240
0.70	−0.29582	−0.30337	−0.30422	−0.30775	−0.30597	−0.30652	−0.30626
0.80	−0.34855	−0.36411	−0.36305	−0.37001	−0.36576	−0.36705	−0.36775
0.90	−0.40651	−0.43671	−0.43151	−0.44526	−0.43613	−0.43875	−0.44153
1.00	−0.47182	−0.53030	−0.51592	−0.54441	−0.52426	−0.52995	−0.53741
1.20	−0.64163	−0.91247	−0.80937	−0.99139	−0.85244	−0.88843	−0.94429
1.40	−0.94883	−1.97070	−1.69170	−2.12480	−1.85260	−1.94320	−2.01490
1.60	−1.69320	−2.78490	−2.57820	−2.91910	−2.73020	−2.79250	−2.80400
1.80	−2.51140	−3.36650	−3.19100	−3.49680	−3.34220	−3.39270	−3.38360
2.00	−3.10820	−3.83410	−3.67330	−3.96640	−3.82850	−3.87320	−3.85450
2.20	−3.58160	−4.23270	−4.07980	−4.36950	−4.24060	−4.28210	−4.24900
2.40	−3.98110	−4.58400	−4.43570	−4.72640	−4.60270	−4.64230	−4.59770
2.60	−4.33080	−4.90050	−4.75490	−5.04900	−4.92810	−4.96660	−4.91250
2.70	−4.49140	−5.04830	−4.90360	−5.19990	−5.07980	−5.11790	−5.06230

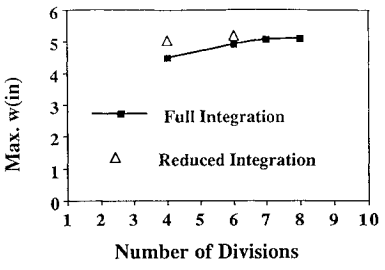

Fig. 4 Convergence study of the present 16-node surface-parallel quadratic element in modeling a clamped cross-ply [0/90] cylindrical panel.

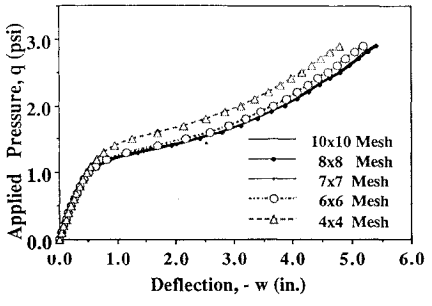

Fig. 5 Load-deflection (equilibrium) paths for different meshes of the 16-node element for a clamped cross-ply [0/90] cylindrical panel.

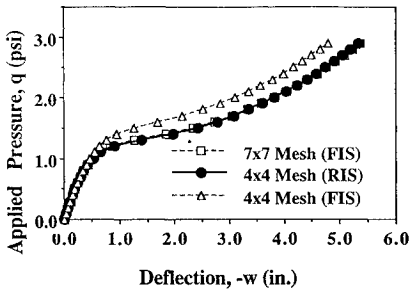

Fig. 6 Comparison of reduced and full integration schemes for convergence rate in computation of equilibrium path of a clamped cross-ply [0/90] cylindrical panel.

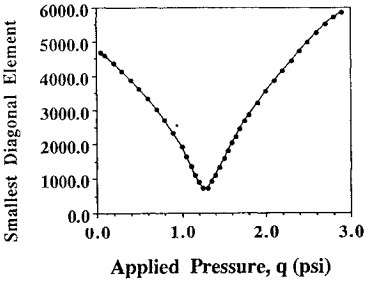

Fig. 7 Variation of the current stiffness parameter of a clamped [0/90] cylindrical panel with the applied load.

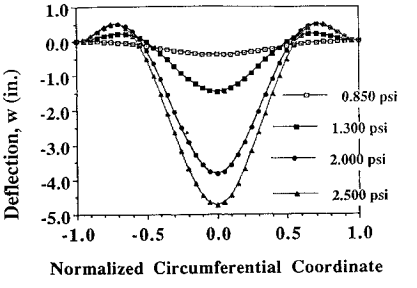

Fig. 8 Variation of the deflection of a clamped cross-ply [0/90] cylindrical panel along the centerline parallel to the θ axis (i. e., $x = 0$ plane) for the different load steps.

A further illustration of the nonlinear behavior of this panel is provided in Fig. 7, which shows the variation of the smallest diagonal element of the factorized stiffness matrix with the applied loading. Stiffness reduction continues until a minimum value (i.e., point M, 15.2% of the initial tangent stiffness) is reached at approximately $P_r = 1.250$ psi, which corresponds to the point of inflection on the load-displacement curve in Fig. 5. For any further increase of the load, the stiffness of the panel starts to rise due to the stiffening effect of longitudinal tensile stresses being developed. Figure 8, which shows variation of the deflection along the centerline parallel to the θ axis (i.e., $x = 0$ plane) for four different load steps, reveals that the deflected region is restricted to the central portion of the panel during the initial load steps. However, it spreads to the boundary regions with the increase of the applied pressure.

Finally, the accuracy of the von Kármán nonlinear strain approximation (KNSA) in the advanced nonlinear regime of the composite [0/90] cylindrical panel, characterized by large extensional

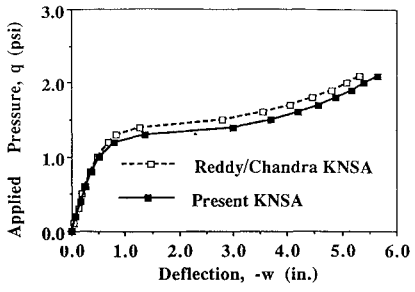

Fig. 9 Comparison of the present von Kármán nonlinear solution with its counterpart due to Reddy and Chandrasekhara for a clamped cross-ply [0/90] cylindrical panel under uniform loading.

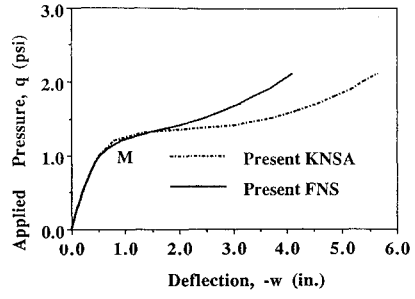

Fig. 10 Comparison of the present fully nonlinear solution with its von Kármán counterpart for a clamped cross-ply [0/90] cylindrical panel under uniform loading.

strain, is investigated. First, the numerical results of the thin/shallow composite cylindrical panel, shown in Fig. 3, using the KNSA are obtained for the purpose of comparison with their counterparts computed by Reddy and Chandrashekhara.[10] To achieve this end, the nonlinear strain components given by Eq. (8) are employed. Reddy and Chandrashekhara[10] have extended Sanders' theory for transversely inextensible shell to account for constant shear deformation through the entire laminate thickness and used the von Kármán nonlinear strain approximation to develop an assumed displacement finite element model for the analysis of a laminated composite panel under uniformly distributed loading. The present KNSA-based results shown in Fig. 9 are expected to be more accurate than those of Reddy and Chandrashekhara,[10] because the former accounts for a higher degree of shear flexibility (in addition to transverse extensibility) incorporated in the layerwise linear displacement distribution theory (LLDT), as compared with the latter, which is based on the first-order shear deformation theory (FSDT). Additionally, the KNSA employed by Reddy and Chandrashekhara[10] ignores the nonlinear terms in the expressions for the interlaminar shear strains, ε_{13} and ε_{23}, involving derivatives of the transverse displacement w with respect to thickness coordinate z that result in greater transverse shear flexibility. These differences may be responsible for causing the present KNSA solution to yield higher central deflection values in the advanced nonlinear regime even for a thin cross-ply [0/90] panel, assuming that the results presented by Reddy and Chandrashekhara[10] have fully converged.

For the laminated composite cylindrical panel (even for a very thin and shallow panel, e.g., $2a/h = 100$, $R/h = 1000$), it is observed that the fully nonlinear strain (FNS)-based solution is slightly higher than its present KNSA counterpart in the part of the equilibrium path around the inflection point M shown in Fig. 10. This can be explained by the fact that the difference between the magnitudes of the circumferential compressive stress and its longitudinal tensile counterpart is slightly larger in the case of the FNS as compared with the KNSA. The preceding difference accounts for slight lowering of the total stiffness in the case of the FNS as compared with its KNSA counterpart. In the advanced nonlinear regime, the KNSA-based solution is higher than the corresponding FNS by as much as 27.3% of maximum displacement just for the opposite reason. In other words, larger tensile stresses develop in the longitudinal and circumferential directions in the advanced nonlinear regime when the FNS is used, as compared with the KNSA. These stresses are responsible for enhancement of the geometric stiffness and, consequently, the total stiffness. In conclusion, severe distortions involving 1) extensional strains due to the rigidly clamped boundary conditions and 2) derivatives of the in-plane displacements u and v with respect to surface-parallel coordinates, x and θ, that result in greater geometric stiffness, are responsible for the difference between the computed FNS-based solution and its KNSA counterpart in the advanced postbuckling regime for the composite cylindrical panel investigated here.

VII. Summary and Conclusions

A total Lagrangian-type nonlinear analysis for prediction of large deformation behavior of thick laminated composite cylindrical shells and panels is presented. The analysis accounts for fully nonlinear kinematic relations, in contrast to the commonly used von Kármán nonlinear strain approximation (KNSA), so that stable equilibrium paths in the advanced nonlinear regime can be accurately predicted. The present nonlinear finite element solution methodology, based on the hypothesis of layerwise linear displacement distribution through thickness (LLDT), yields a degenerated multilayer cylindrical shell element. The present surface-parallel quadratic (16-node) layer element, with 8 nodes on each of the top and bottom surfaces of each layer, has been implemented in conjunction with full and reduced numerical integration schemes to efficiently model both thin and thick shell behavior. The modified Newton–Raphson iterative scheme with Aitken acceleration factors is used to obtain hitherto unavailable numerical results corresponding to fully nonlinear behavior of the analyzed panels. A two-layer [0/90] thin/shallow clamped cylindrical panel is investigated to assess the convergence rates for full and reduced integration schemes, and to check the accuracy of the present degenerated cylindrical shell layer element. Accuracy of the von Kármán nonlinear approximation (KNSA), currently employed in many investigations on buckling/postbuckling behavior of thin shells, is assessed, in the case of laminated thin shells and panels, by comparing the numerical results obtained using this approximation with those due to fully nonlinear kinematic relations, especially in the advanced stable postbuckling regime. What follows is a list of useful conclusions drawn from the present investigation:

1) Numerical results on the effect of the order of numerical integration, such as reduced and full samplings, on the convergence rate clearly indicate that the use of the reduced integration scheme, in general, accelerates the rate of convergence of displacements in thin and moderately thick shells.

2) Stiffness reduction of a two-layer [0/90] clamped cylindrical panel continues until a mimimum is reached at 15.2% of the initial tangent stiffness, which corresponds to an inflection point on the load displacement curve. This is followed by a rise in stiffness due to the stiffening effect of tensile stresses developed in both the longitudinal and circumferential directions.

3) Numerical results on a two-layer [0/90] clamped cylindrical panel further show that the von Kármán nonlinear strain approximation (KNSA) yields a significantly higher (in the range of 27.3%) central deflection, compared with its fully nonlinear strain (FNS) counterpart in the advanced nonlinear regime.

Appendix: Definition of Some Matrix Operators

The differential operator matrix $[\boldsymbol{B}_{LL}]$ referred to in Eq. (16a) is given as follows:

$$[\boldsymbol{B}_{LL}] = \begin{bmatrix} \dfrac{\partial}{\partial x} & 0 & 0 \\ 0 & \dfrac{1}{g_\theta}\dfrac{\partial}{\partial \theta} & \dfrac{1}{g_\theta} \\ 0 & 0 & \dfrac{\partial}{\partial z} \\ 0 & \dfrac{\partial}{\partial z} - \dfrac{1}{g_\theta} & \dfrac{1}{g_\theta}\dfrac{\partial}{\partial \theta} \\ \dfrac{\partial}{\partial z} & 0 & \dfrac{\partial}{\partial x} \\ \dfrac{1}{g_\theta}\dfrac{\partial}{\partial \theta} & \dfrac{\partial}{\partial x} & 0 \end{bmatrix} \tag{A1}$$

The differential operator matrix $[\boldsymbol{B}_{NL}]$ referred to in Eq. (16b) is given as follows:

$$[\boldsymbol{B}_{NL}] = \{[\boldsymbol{B}_{NL1}][\boldsymbol{B}_{NL2}][\boldsymbol{B}_{NL3}]\} \tag{A2}$$

where

$$[\boldsymbol{B}_{NL1}] = \begin{bmatrix} R_{11}\dfrac{\partial}{\partial x} \\ \dfrac{R_{21}}{g_\theta}\dfrac{\partial}{\partial \theta} \\ R_{31}\dfrac{\partial}{\partial z} \\ \dfrac{R_{31}}{g_\theta}\dfrac{\partial}{\partial \theta} + R_{21}\dfrac{\partial}{\partial z} \\ R_{31}\dfrac{\partial}{\partial x} + R_{11}\dfrac{\partial}{\partial z} \\ \dfrac{R_{11}}{g_\theta}\dfrac{\partial}{\partial \theta} + R_{21}\dfrac{\partial}{\partial x} \end{bmatrix} \tag{A3a}$$

$$[\boldsymbol{B}_{NL2}] = \begin{bmatrix} R_{12}\dfrac{\partial}{\partial x} \\ \dfrac{1}{g_\theta}\left(R_{22}\dfrac{\partial}{\partial \theta} - R_{23}\right) \\ R_{32}\dfrac{\partial}{\partial z} \\ R_{22}\dfrac{\partial}{\partial z} + \dfrac{R_{32}}{g_\theta}\dfrac{\partial}{\partial \theta} - \dfrac{R_{33}}{g_\theta} \\ R_{32}\dfrac{\partial}{\partial x} + R_{12}\dfrac{\partial}{\partial z} \\ R_{22}\dfrac{\partial}{\partial x} + \dfrac{R_{12}}{g_\theta}\dfrac{\partial}{\partial \theta} - \dfrac{R_{13}}{g_\theta} \end{bmatrix} \tag{A3b}$$

$$[\boldsymbol{B}_{NL3}] = \begin{bmatrix} R_{13}\dfrac{\partial}{\partial x} \\ \dfrac{R_{23}}{g_\theta}\dfrac{\partial}{\partial \theta} + \dfrac{R_{22}}{g_\theta} \\ R_{33}\dfrac{\partial}{\partial z} \\ \dfrac{R_{32}}{g_\theta} + \dfrac{R_{33}}{g_\theta}\dfrac{\partial}{\partial \theta} + R_{23}\dfrac{\partial}{\partial z} \\ R_{33}\dfrac{\partial}{\partial x} + R_{13}\dfrac{\partial}{\partial z} \\ R_{23}\dfrac{\partial}{\partial x} + \dfrac{R_{13}}{g_\theta}\dfrac{\partial}{\partial \theta} + \dfrac{R_{12}}{g_\theta} \end{bmatrix} \tag{A3c}$$

in which

$$\{R_{ij}\} = [\boldsymbol{B}_{NN}]\{\bar{v}\} \tag{A4}$$

with

$$\{R_{ij}\} = \{R_{11}\ \ R_{12}\ \ R_{13}\ \ R_{21}\ \ R_{22}\ \ R_{23}\ \ R_{31}\ \ R_{32}\ \ R_{33}\}^T \tag{A5}$$

$$\{\bar{v}\} = \{\bar{u}\quad \bar{v}\quad \bar{w}\}^T \tag{A6}$$

where the components of the vector $\{\bar{v}\}$ are known displacements at time t. Finally, the differential operator matrix $[\boldsymbol{B}_{NN}]$ referred to in Eqs. (16c) and (A4) is given as follows:

$$[\boldsymbol{B}_{NN}] = \begin{bmatrix} \dfrac{\partial}{\partial x} & 0 & 0 & \dfrac{1}{g_\theta}\dfrac{\partial}{\partial \theta} & 0 & 0 & \dfrac{\partial}{\partial z} & 0 & 0 \\ 0 & \dfrac{\partial}{\partial x} & 0 & 0 & \dfrac{1}{g_\theta}\dfrac{\partial}{\partial \theta} & -\dfrac{1}{g_\theta} & 0 & \dfrac{\partial}{\partial z} & 0 \\ 0 & 0 & \dfrac{\partial}{\partial x} & 0 & \dfrac{1}{g_\theta} & \dfrac{1}{g_\theta}\dfrac{\partial}{\partial \theta} & 0 & 0 & \dfrac{\partial}{\partial z} \end{bmatrix}^T \tag{A7}$$

References

[1]Koiter, W. T., "Elastic Stability and Post-Buckling Behavior," *Nonlinear Problems*, edited by R. E. Langer, Univ. of Wisconsin Press, Madison, WI, 1963.

[2]Seide, P., and Chaudhuri, R. A., "Triangular Finite Element for Analysis of Thick Laminated Shells," *International Journal for Numerical Methods in Engineering*, Vol. 27, No. 8, 1987, pp. 1563–1579.

[3]Hsia, R. L., and Chaudhuri, R. A., "Geometrically Nonlinear Analysis of Cylindrical Shells Using Surface-Parallel Quadratic Elements," *Computers and Structures* (to be published).

[4]Noor, A. K., and Hartley, S. J., "Nonlinear Shell Analysis Via Mixed Isoparametric Elements," *Computers and Structures*, Vol. 7, No. 5, 1977, pp. 615–626.

[5]Chang, T. Y., and Sawamiphakdi, K., "Large Deformation Analysis of Laminated Shells by Finite Element Method," *Computers and Structures*, Vol. 13, Nos. 1–3, 1981, pp. 331–340.

[6]Sarhangnezhad, A. A., "Nonlinear Formulation of the Multilayer General Shell Finite Element," Ph.D. Dissertation, Dept. of Civil Engineering, Univ. of Southern California, Los Angeles, CA, 1982.

[7]Bathe, K. J., and Bolourchi, S., "A Geometric and Material Nonlinear Plate and Shell Element," *Computers and Structures*, Vol. 11, Nos. 1–2, 1980, pp. 23–48.

[8]Epstein, M., and Glockner, P. G., "Nonlinear Analysis of Multilayered Shells," *International Journal of Solids and Structures*, Vol. 13, No. 11, 1977, pp. 1081–1089.

[9]Palazzotto, A. N., and Witt, W. P., "Formulation of a Nonlinear Compatible Finite Element for the Analysis of Laminated Composites," *Computers and Structures*, Vol. 21, No. 6, 1985, pp. 1213–1234.

[10]Reddy, J. N., and Chandrashekhara, K., "Nonlinear Analysis of Laminated Shells Including Transverse Shear Strains," *AIAA Journal*, Vol. 23, No. 3, 1985, pp. 440, 441.

[11]Green, A. E., and Zerna, W., *Theoretical Elasticity*, Clarendon Press, Oxford, England, UK, 1968.

[12]Seide, P., *Small Elastic Deformation of Thin Shell*, Noordhoff, International, Leyden, The Netherlands, 1975.

[13]Bathe, K. J., *Finite Element Procedures in Engineering Analysis*, Prentice–Hall, Englewood Cliffs, NJ, 1982.

[14]Strang, G., and Fix, G. J., *An Analysis of the Finite Element Method*, Prentice–Hall, Englewood Cliffs, NJ, 1973.

[15]Stroud, A. H., and Secrest, D., *Gaussian Quadrature Formulas*, Prentice–Hall, Englewood Cliffs, NJ, 1966.